Human serum albumin capsulated hydrophobic carbon nanodots as staining agent on HeLa tumor cell

by Mochamad Zakki Fahmi

Submission date: 01-Sep-2021 08:43PM (UTC+0800)
Submission ID: 1639427472
File name: uman_serum_albumin_capsulated_hydrophobic_carbon_nanodots_as.pdf (1.96M)
Word count: 6183
Character count: 32923

Materials Chemistry and Physics 239 (2020) 122266

Contents lists available at ScienceDirect

Materials Chemistry and Physics

journal homepage: www.elsevier.com/locate/matchemphys

Human serum albumin capsulated hydrophobic carbon nanodots as staining agent on HeLa tumor cell

Mochamad Zakki Fahmi [a,*], Denika Liyan Nor Wibowo [a], Satya Candra Wibawa Sakti [a], Hwei Voon Lee [b], Isnaeni [c]

[a] Department of Chemistry, Faculty of Science and Technology, Universitas Airlangga, Surabaya, 60115, Indonesia
[b] Nanotechnology and Catalysis Research Centre, Institute of Postgraduate Studies (IPS), University of Malaya, Kuala Lumpur, 50603, Malaysia
[c] Research Center of Physics, Indonesian Institute of Sciences, South Tangerang, Banten, 15314, Indonesia

HIGHLIGHTS

- Human serum albumin capsulated the hydrophobic carbon dots and phase transferred it to be hydrophilic nanoparticle.
- Conjugation of CDs with HAS performs good stability and non toxic.
- The CDs-HSA perform specific targeting on tumor cell, as well as significant fluorescence signal compared with bare CDs.

GRAPHICAL ABSTRACT

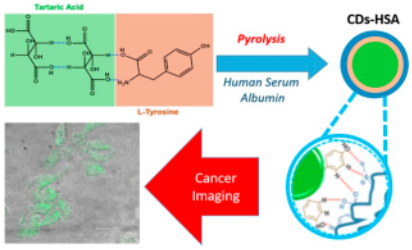

ARTICLE INFO

Keywords:
Hydrophobic carbon nanodots
Human serum albumin
HeLa
Staining agent
Nanoparticle

ABSTRACT

The hydrophobic carbon nanodots (CDs) are promising nanoparticles to develop due to its uniformly size, good photoluminescence properties, and easy surface-modification. Highly photoluminescent hydrophobic CDs have been synthesized by carbonization of tartaric acid–L-tyrosine precursors. These hydrophobic CDs showed uniformly size distribution and exhibited strong-blue emission under UV irradiation. Further surface modification using human serum albumin (HSA) lead to the formation of hydrophilic CDs-HSA within low toxicity and good colloidal stability over varied pH and high ionic strengths. Various spectroscopies characterizations were done to analyze the morphological and chemical composition of both CDs and CDs-HSA. Further improvement analyses on cytotoxicity and confocal laser microscopy (CLSM) upon HeLa tumor cell suggested that the designed CDs-HSA was effective to be applied as staining agent against tumor cells.

1. Introduction

In the past two decades, the photoluminescent nanoparticle have exhibited extensive application, from optical analysis to biological sensing [1,2]. Carbon nanodots (CDs) as one kind of photoluminescent nanoparticle possessing excellent properties such as low toxicity, enable for surface modification, resistance to photobleaching, and good biocompatibility [3–5]. The most synthesized CDs are hydrophilic in nature with the size below 10 nm [6]. The common synthesize of CDs has taken on two approaches, the first is top-down methods, which the

* Corresponding author.
E-mail address: m.zakki.fahmi@fst.unair.ac.id (M.Z. Fahmi).

https://doi.org/10.1016/j.matchemphys.2019.122266
Received 3 May 2019; Received in revised form 3 October 2019; Accepted 7 October 2019
Available online 12 October 2019
0254-0584/

CDs are formed from larger carbon structure [7]. The synthesis that include on this method are arc discharge [8], electrochemical synthesis [9], and laser ablation [10]; whereas the combustion or thermal synthesis [11], microwave irradiation [12], and hot injection [13] are belonging to bottom-up method. These methods specifically performed preeminence on producing CDs, but remain general limitations, such as the use of concentrate or toxic chemicals, complicating reaction process, uncontrollable CDs size distribution, low optical properties and low yield product [14]. To overcome those problems, many researchers report application carbonization, as part bottom-up method, that giving thermal, even pressure treatment, on carbon precursors. The carbonization process was proven on granting production of CDs with narrow size distribution, a simple partway, and many option on chemical precursor [15,16]. By choosing the thermal condition and aromatic framework of precursors, the composition and properties of yielded CDs can also be tuned easily [17].

Development of hydrophobic CDs or graphene quantum dots, so far, was mainly addressed to any application outer biological fields. This phenomena was finely understood due to water solubility became principally requirement for material to freely enter on biological circumstances [18]. Although hydrophobic CDs were not preferable to be developed, these kind nanoparticles showed advantages, such as higher optical properties, well-controlled size, easiness on its purification, and available as powder [19]. Therefore, efforts on manipulating CDs solubility became crucial factor its synthesis process.

The modifications on the surface of CDs with coating materials are needed to enhance its water solubility, the biocompatibility, and stability for application on living cells [20]. Compared to other molecules, proteins are more preferable as a coating material for CDs modification due to their biocompatibility, stability, and biodegradability. Serum albumin proteins were ideal candidate as coating materials for fabricating the hydrophilic CDs. On our previous report, it was developed multifunctional nanocarriers using bovine serum albumin (BSA), which act as a coating for the hybrid nanoparticles [21]. BSA is protein with various functional groups that could create bond with other proteins [22], even with nanoparticles [23]. Human serum albumin (HSA) is another kind of serum albumin, which found in blood plasma and cerebrospinal solution in human body. HSA molecules also have hydrophobic pockets which can bound the hydrophobic molecules and transport them [24]. This HSA were widely developed as a coating agent for nanoparticles in various research about cancer imaging and therapy due to its ability to drive nanoparticle specific targeting on tumor cell through passive targeting (EPR effect) and active targeting via attractive binding with both secreted protein acidic and rich in cysteine (SPARC) and the gp60 transcytosis pathways [25,26].

The previous research reported that HSA molecules can encapsulated the hydrophobic IR780 dye for imaging, photodynamic, and photothermal therapy of cancer [27]. Nowadays, the HSA-based nanoparticulate Paclitaxel (PTX) drug, named Abraxane™, have been commercially available as drug for breast cancer [28,29]. Therefore, the utilizing of HSA to form hydrophilic CDs-HSA for further application in live cells is more suitable. In this present work, we reported the synthesis of hydrophobic CDs along with its modification using a simple and low-cost approach. We develop carbonization process using commercial tartaric acid as precursors to synthesize CDs and L-tyrosine molecules as surface-passivizing agents to produce hydrophobic CDs. Further coating of synthesized CDs by using HSA molecules were done to generate biological compatibility against HeLa cells. One of highlighted aspect on present study is improvement fluorescent capability of obtained CDs, which drive the CDs as staining agent of cancer. These CDs have highly fluorescent with blue emission under UV irradiation ($\lambda = 365$ nm) and also possessed low toxicity even in high concentration, thus indicated the ability of synthesized CDs for bioimaging and biosensing applications [30,31]. Beside characterization of obtained CDs, further observation on bioimaging capability of CDs through confocal assessment was important part to be investigated.

2. Experimental procedures

2.1. Materials

Tartaric acids (99.5%), L-tyrosine (99%), HSA (≥97%), Dulbecco's Modified Eagle Medium (DMEM) and ethanol (99.8%) were purchased from Sigma-Aldrich (Milwaukee, WI, USA). Monosodium (2-(2-metoksi-4-nitrofenil)-3-(4-nitrofenil)-5-(2,4-disulfofenil)2H-tetrazolium) salt (WST-8 or cck-8, 97.5%) was purchased from Dojindo Molecular Technology Inc. (Kumamoto, Japan). Hydrogen chloride (HCl, 37%) and Sodium hydroxide (NaOH, 98.5%) were purchased from Bratachem (Surabaya, Indonesia). All chemicals were directly used without next purification.

2.2. Synthesis of nanoparticles CDs

The CDs were synthesized according to previously procedure proposed by Gude et al. with some modifications [19]. Experimentally, L-tyrosine was firstly dissolved in HCl to give an acidified solution under its isoelectric pH, 5.66 [32]. This solution was added drop-wise to an aqueous solution of tartaric acid under constant stirring with molar ratio of tartaric acid and L-tyrosine was 1:4. The mixture was heated to 130 °C until all the water was evaporated. The resulting colorless powder were pyrolyzed at 220 °C for 30 min in a furnace. Dark-brown solid of CDs were obtained after this pyrolysis process and were used in the next step. Hydrophilic CDs also was made following above method with the absent of L-Tyrosine. To cytotoxicity purpose, hydrophilic CDs also prepared following above procedure with the absence of L-Tyrosine. The pyrolyzed tartaric acid was further dissolved with NaOH solution before neutralized its pH and marked as hydrophilic CDs.

2.3. Synthesis of CDs-HSA

The synthesized CDs (1.5 mg) were dissolved in 1 mL ethanol and resulting yellow-brownish clear solution. This solution was added to 0.1612 mM of HSA, which dissolve in 10 mL DI water. This mixture was subsequently ultrasonicated for 2 min using Ultrasonic Homogenizer (JY 92-IIDN, China) and kept the temperature to avoid coagulation of HSA. The ultrasonication process was operated at power of 80% (1000 WW, 20 kHz) until the ethanol and aqueous phase were homogenously mixed. After the process, the solution was left at room temperature for 30 and further purified using dialysis membrane MWCO 40 kDs (Orange Scientific, Belgium) for 24 h to remove side products and incapsulated CDs.

2.4. Characterization

The crystal structure CDs were determined by X-ray diffraction (XRD) Ultima IV (Rigaku, USA) with rotating anode source the Cu $K_{\alpha 1}$ line ($\lambda = 1{,}54$ Å) and 18 kW. Fourier transform infrared (FTIR) spectra were measured on IRTracer-100 spectrometer (Shimadzu, Japan) using KBr pellets of the dried CDs samples. Atomic Force Microscopy (AFM) images of CDs were acquired using AFM5500 M instrument (Hitachi Co., Japan) at room temperature. Dynamic light scattering (DLS) analysis of CDs-HSA were conducted using a Zetasizer Nanoseries (Malvern, USA) with He–Ne laser operating at $\lambda = 633$ nm. UV-Vis absorption spectra were measured using a Shimadzu 1800 spectrophotometer. The PL spectra were carried out by using a PerkinElmer LS 55 spectrofluorometer equipped with 20 kW xenon lamp. Raman analysis was performed using MRS-320 Raman Instrument system (Horiba Ltd., Japan). Stability of CDs assessed by TB1 turbidimeter (Velp Scientifica, Italy).

2.5. Cytotoxicity and confocal evaluation of CDs-HSA

The cytotoxicity of CDs-HSA was evaluated by assess HeLa tumor cells viability with WST-8 assay. The tumor cells are previously cultured on DMEM medium with FBS and stored at incubator with maintained

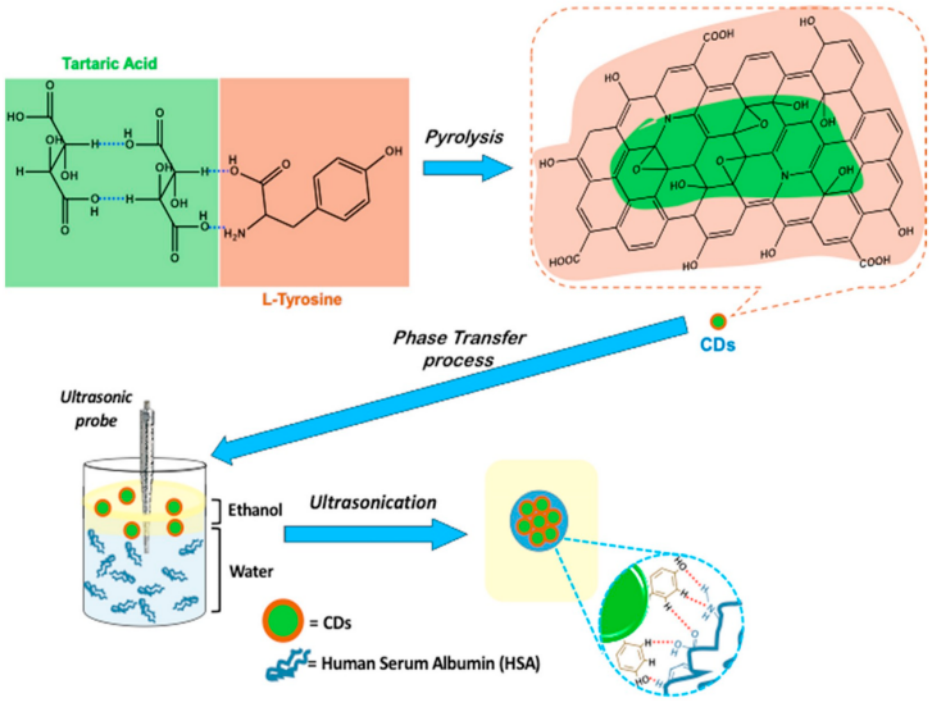

Scheme 1. Schematic synthesis of CDs and its phase transfer process by HSA capsulations.

condition on humidified 5% CO_2 and atmosphere at 37 °C. On the cultivating day, HeLa cells were seeded in a 24-well plate with density of 9×10^4 cells/μL and incubated for 24 h to allow cell attach on bottom flask and grow. After 24 h, cells were washed with PBS, new medium and varied concentrations of CDs-HSA were added to each well. After left the cell for 24 h on the incubator, all of the well is added with 10 μL

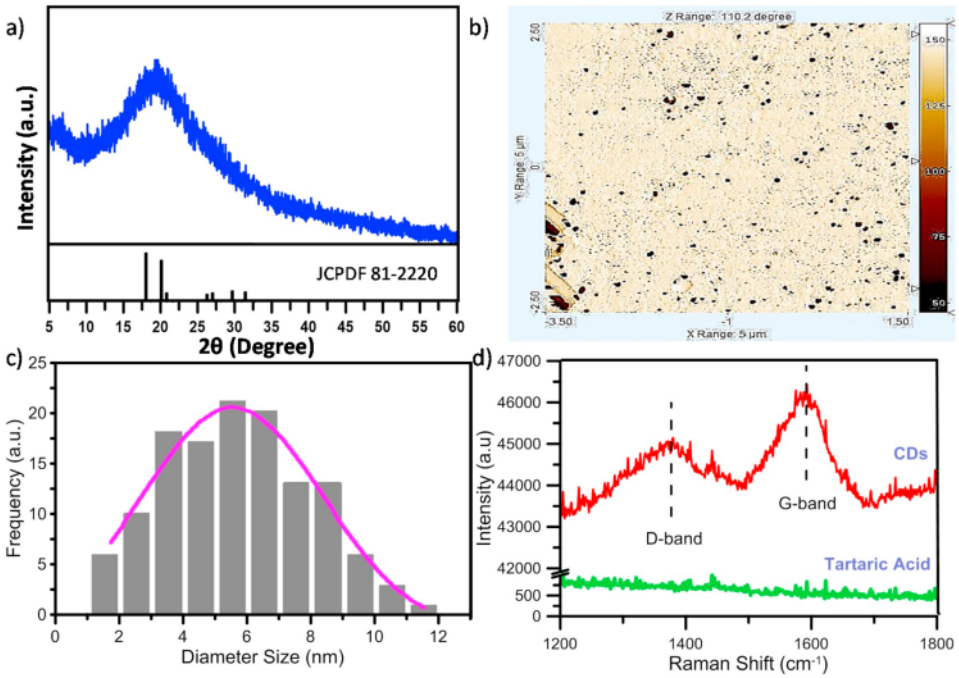

Fig. 1. (a) Diffractogram of CDs, (b) AFM image of CDs, (c) diameter distribution of CDs according to AFM analysis, and (d) Raman spectra of CDs and tartaric acid.

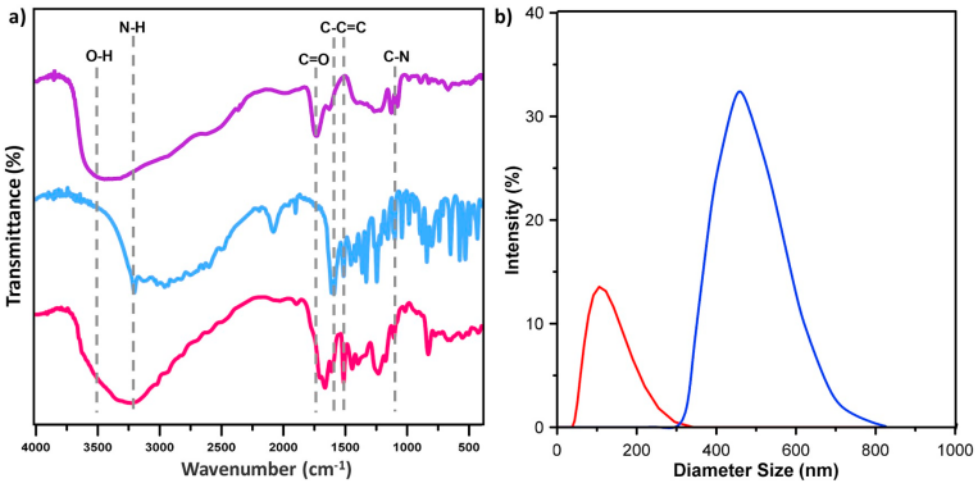

Fig. 2. (a) FTIR spectra of tartaric acid (purple line), L-tyrosine (blue line), and CDs (red line), with corresponding functional group of each compound, and (b) Diameter of HSA (blue line) and CDs-HSA (red line) by DLS analysis. (For interpretation of the references to color in this figure legend, the reader is referred to the Web version of this article.)

WST-8 reagents, then incubated in CO_2 incubator at 37 °C for 2 h. The absorbance of the formazan in each well were measured using ELISA iMark microplate reader (Bio-Rad, USA) at the wavelength of 450 nm. This assay is based on a reduction of 2-(2-methoxy-4-nitrophenyl) -3-(4-nitrophenyl) -5-(2,4-disulfophenyl) -2H tetrazolium monosodium salt (WST-8) by the living cells to obtained water-soluble formazan dye. The amount of formazan that generated by the living cells was proportional to the number of live cells. In order to give proportional comparison, cytotoxicity data of CDs-HSA was compared with hydrophilic CDs prepared above.

On the Confocal Laser Scanning assessment, the HeLa cells is incubated with sample (300 μL) for 60 min after seeded in a 6-well plate with DMEM medium and incubated for 24 h the treated cells were then washed with PBS solution and fixed with 70% alcohol for 10 min. Fluorescence images were obtained from the cell with 63 × 1.32 NA oil immersion objective using confocal TCS SP2 (Leica Microsystems, USA) equipped with inverted microscope and inline Ar (488 nm) and He–Ne (503–680 nm and 588 nm) lasers.

3. Results and discussion

3.1. Synthesis and characterization of nanoparticles CDs

The present study, CDs as carbogenic nanomaterial were synthesized via carbonization method, where tartaric acid and L-tyrosine were main precursors. Tartaric acid was acts as source of CDs core, while L-tyrosine as passivizing agent covering the core. As bottom-up method, carbonization on high temperature allowing association of tartaric acid molecules bring out the chemical binding and releasing water simultaneously, as shown on Scheme 1. The dark-brown solid-like were produced during this carbonization process indicated that the formation of CDs were through dehydration and formation of amide bond [33]. On this system, the dehydration process is not only work in between tartaric acid, but also L-tyrosine tartaric acid. The higher L-tyrosine concentration enhance potency of this molecule covering tartaric acid-based CDs and make the unity become hydrophobic as initial properties of L-tyrosine. This statement was proven by insolubility of obtained CDs on water, but highly solubility on organic solvent such as ethanol, acetone, and DMSO etc.

CDs formation was first confirmed from XRD analysis, as shown at Fig. 1a. The XRD spectrum exhibits a broad peak and the crystallinity was observed at 2θ about 19.18° and confirmed with corresponding to JCPDS 81-2220 for carbon nanoparticles. This finding was on good agreement with Sahu et al. (2012) reported crystallinity of their CDs, which significantly appear at 19.1° [34]. The analyzed peak (19.18°) was correspond to an interlayer spacing (*d*-spacing) of about 0.4 nm, which higher than of the bulk graphite (002) *d*-spacing (0.33 nm) [19,34]. This confirms the amorphous nature of carbon dots due to the increasing of oxygen containing group located at the CDs surface [35]. Using Scherer equation, XRD result also confirms the CDs crystal size. With FWHM value of CDs at 19.18° is 14.5388, and was converted to crystallite size about 0.10 nm. This size information is further supported by AFM data on Fig. 1b showing where these nanoparticles were found with spherical in shape, similar with previous report [36]. A histogram from the AFM result (Fig. 1c) indicated that CDs have an average size about 5.50 nm and some having size over 10 nm. The Raman spectra on Fig. 1d confirms the structure of obtained CDs. Compared with spectrum of tartaric acid, the spectrum of CDs particularly appears a band at 1352 cm^{-1} referring to carbon atom scattering on the sp^3-hybridization, so called as D band. The other band at 1579 cm^{-1} was also identified as G band for carbon scattering on sp^2 position of the CDs. On comparison analysis of D to G bands intensity (I_D/I_G ratio), it founded that the ratio was 0.9. This ratio value on past report stated the purity and the graphite order of CDs and graphite based material [37], where the ratio value below than one indicated good purity of material on emerging graphene or graphene like structure. It could be seen that the Raman data supported XRD data on prove carbogenic crystal structure of CDs.

3.2. Synthesis and characterization of nanoparticles CDs-HSA

In order to make the CDs well dissolve on water, we next capsulate the hydrophobic CDs with HSA protein through phase transferring process (Scheme 1). On the first step, the aqueous solution of HSA was mixed with CDs dissolved in ethanol. It has been reported that HSA protein possesses three homologous domains, which each domain consisting 2 sub domains (A and B). It was reported that the particular subdomain (IB) of HSA could bind to wide variety of drug and any nonpolar molecules [24,38]. Thus, on the polar solvent, HSA performs hydrophobic cavities as core of these macromolecules and we speculate to expect that the cavities will be the suitable place for the hydrophobic CDs. Furthermore, to push the CDs into the hydrophobic core of HSA, the ultrasonic treatment was applied. This wave provides harmonic

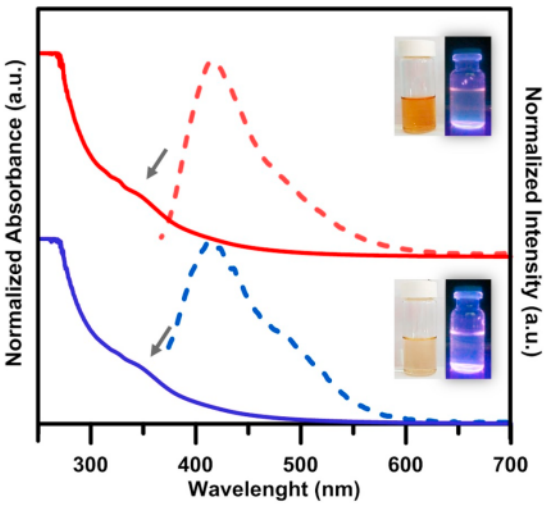

Fig. 3. UV–Vis spectra of CDs and CDs-HSA, insert: photograph of CDs and CDs-HSA under visible light (left) and under 365 nm UV light (right). The arrow at UV–Vis spectra indicated the exciton peaks of CDs.

pressing and expanding force to HSA, once the macromolecule gets the expanding force, the obstacle for CDs to reach the hydrophobic core of HSA is minimized and CDs be capsulated with HSA on water phase.

To prove the capsulation process, FTIR spectroscopy is carried out with comparing analysis of the functional groups of CDs, tartaric acid and L-tyrosine (Fig. 2a). The FTIR spectra of tartaric acid clearly showed adsorption peaks at 3414 cm^{-1} (O–H), 2980 cm^{-1} (C–H), 1734 cm^{-1} (C═O), and 1215 cm^{-1} (C–O). Moreover, L-tyrosine is indicated by peaks at 3205–3128 cm^{-1} (–NH_2), 3040 cm^{-1} (O–H), 1608 cm^{-1} (C═O), 1591–1514 cm^{-1} (–C–C═C–), and 1174 cm^{-1} (C–N). The conjugation of L-tyrosine to tartaric acid was confirmed by the FTIR spectra of CDs which showed adsorption peaks at 3228–3120 cm^{-1} for N–H which overlapped with O–H stretching, 1703 cm^{-1} for C═O, 1610–1514 cm^{-1} for stretching of aromatic carbon atoms (-C-C═C-), and 1174 cm^{-1} for C–N stretching. Another physicochemical analysis using DLS showed the hydrodynamic diameter of CDs after HSA addition (CDs-HSA) was 100.2 nm (Fig. 2 b). The CDs-HSA diameter was larger than corresponding CDs and HSA, respectively, indicating the presence of CDs on HSA molecules.

The optical properties of CDs and CDs-HSA were observed using adsorption and photoluminescence spectroscopy. The UV–Vis spectra for CDs and CDs-HSA showed adsorption at the same wavelength (278 nm) as shown in Fig. 3. The CDs spectra was correlated to the n → π* transition of the C═O and π → π* transition of aromatics C═C. The HSA molecules also had maximum adsorption at 278 nm due to the π → π* transition of its amino acid residues. It was easy to observe that, the adsorption spectrum of CDs-HSA is persistent at the wavelength of 278 nm, with the higher intensity than of CDs solution. Next, the presence of another peak at 345 nm attributes to adsorption of the CDs exciton [39]. This exciton was found at CDs-HSA spectra that confirmed the conjugation of CDs with HSA molecules. The solution of CDs in ethanol showed yellow-transparent color, while aqueous CDs-HSA solution had pale yellow-transparent in daylight. When UV radiation (365 nm) was given to this solution, the colors changes to intense blue, as shown on insert of Fig. 3.

The photoluminescence (PL) spectra of CDs with varied excitation wavelength (340–440 nm) indicating that the CDs had a multicolor photoluminescence emission, where the intensity follows on the excitation wavelength (as shown in Fig. 4). A strong emission peak was identified at 420 nm with the blue-light emission at the excitation

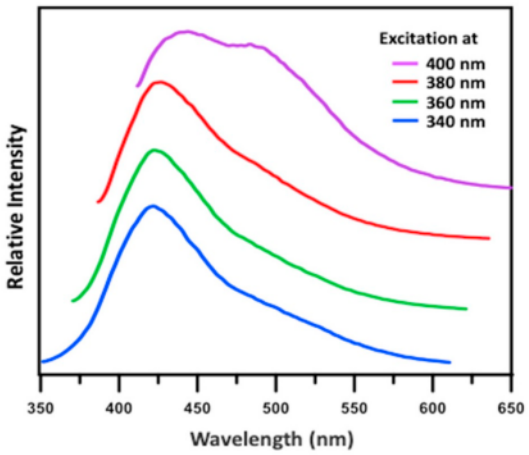

Fig. 4. PL emmision spectra at different excitation wavelength of CDs.

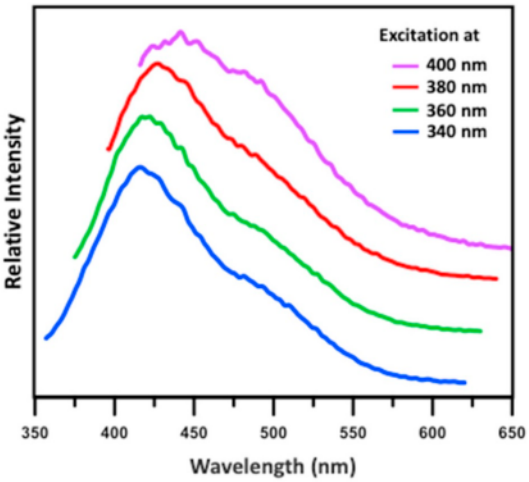

Fig. 5. PL emmision spectra at different excitation wavelength of CDs-HSA.

wavelength of 360 nm. When the higher excitation wavelength was applied, the peak was shifted to a higher wavelength (bathochromic shift). The intensity of this shifted peak also decreases thus the band become broader at visible region.

The PL spectra of CDs-HSA on varied excitation wavelength were shown in Fig. 5. These spectra showed red shift as CDs spectra and also exhibit emission peak at 420 nm with the excitation wavelength of 360 nm. The CDs and CDs-HSA spectra have the same emission and excitation wavelengths, even the CDs-HSA had a lower intensity and broader peak. The phenomena also support previous finding on confirm incorporation of CDs on HSA molecules. The lower intensity of CDs was mainly caused by its lower concentration and covering HSA, that not perform an optical property, will diminish nature emission of CDs. Furthermore, the shifting emissions of CDs, which dependent on excitation wavelength, were affected by complicating oxidation defect on CDs. These defect make unperfected graphene like structure of CDs and contribute to obtain complex orbital states and trap exciton way [40]. These additional states render the emission energy levels follow the excitation level. The various surface functional groups of CDs also affected the PL spectra since it results in a series of emissive traps

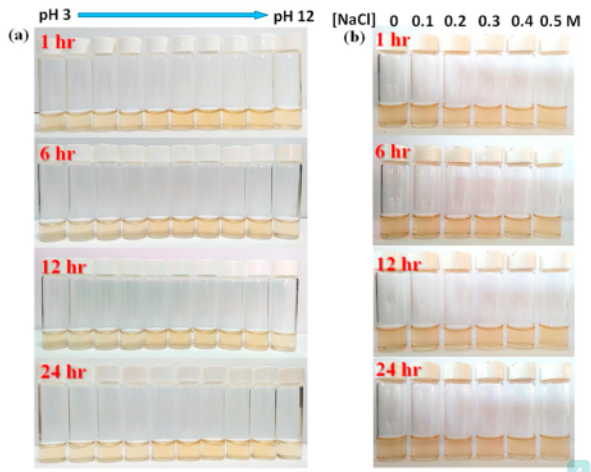

Fig. 6. Colloid stability analysis of CDs-HSA. (a) Photograph of CDs-HSA at different pH value, (b) photograph of CDs-HSA at different NaCl concentration.

between π and π* of C═C aromatics. The CDs illuminate with specific excitation wavelength and the surface energy trap dominates the emission. Once the wavelength was altered, the other surface functional group emissive traps become dominant.

3.3. Colloid stability analysis

Colloidal stability of CDs-HSA was investigated against the variation of pH and ionic strength. The stability was observed by varied time up to 24 h after preparation (Fig. 6a). The unstable CDs-HSA that tended to coagulate was observed at low pH value (pH 3) and higher pH value (pH 11 and 12). Since HSA was present in compendious shape and maintained its origin structure between pH 4 to 9 [41]. As on our report before, the destruction of CDs-HSA designs on low and high pH due to the conformational change and interfered the molecular interaction between HSA and CDs [21]. This altered conformation lead to disruption of hydrophobic and electrostatic interactions of HSA and CDs, leading to the coagulation. This observation was further validated with turbidity measurement of CDs-HSA (Table S1, on Supporting Information), where the coagulation was detected by high turbidity value on pH 3 and pH 11–12 of the sample (the regular range were 2.25–3.31 NTU). Further UV–Vis absorption spectra on varied pH of CDs-HSA (Fig. S1, on Supporting Information) supported previous finding on revealing destruction of this nanoparticle. The spectrum of CDs-HSA at pH 3, pH 11 and pH 12 show irregular spectra.

The colloidal stability test regarding ionic strength were also observed by adding various concentration of NaCl up to 0.5 N. Fig. 6b showed that the CDs-HSA defended its colloidal stability since the expansion of HSA structure can be prevented. The higher NaCl concentration that added to the CDs-HSA, influenced the hydrophobic interaction thus resulting continuous interaction between HSA and CDs [21]. The turbidity data (Table S1, on Supporting Information) of adjusted pH and NaCl on CDs-HSA also supporting Fig. 6, where after 24 h, CDs-HSA with pH value 1–3 and 12–14 perform significantly high turbidity value (over 4.2 NTU). Higher turbidity value indicates aggregation or destruction of CDs-HSA structure due to denaturation of HSA and affecting on precipitation of CDs-HSA. Furthermore, concerning on its application on biological condition, stability evaluation of CDs-HSA also driven on FBS and cell culture DMEM mediums, where turbidity value on those condition was $3{,}77 \pm 0.26$ and 2.88 ± 0.53, respectively, as low as regular CDs-HSA on pH 7 indicating no aggregation performed. These analyses confirmed that CDs-HSA could be used in living

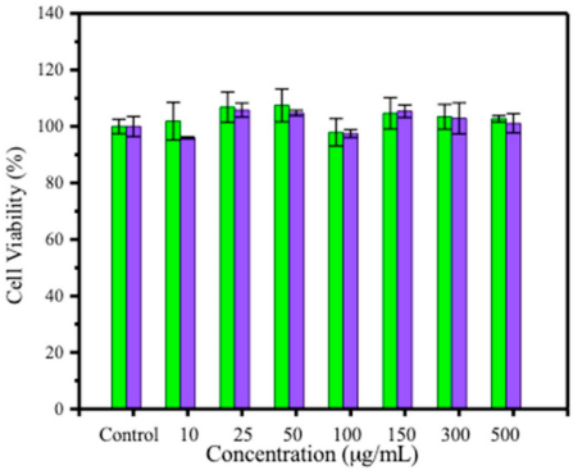

Fig. 7. Cell viability of HeLa tumor cell after 24 h incubation with CDs (green) and CDs-HSA (blue). (For interpretation of the references to color in this figure legend, the reader is referred to the Web version of this article.)

organism, since it showed good colloidal stability under various physiological conditions appropriate in human body (pH range on 4.5 to 8 and ionic strength of blood vascular on 0.15 N).

3.4. Cytotoxicity assay

In order to assess the potential of CDs and CDs-HSA for future biological application, the *in vitro* cytotoxicity assay was conducted using CCK-8 assay in HeLa cells. The absorbance of formazan, which is produced reaction between mitochondrial enzyme succinate dehydrogenase and WST-8 salt, was directly proportional to the number of living cells [42]. After 24 h incubation with HeLa cells, both of CDs and CDs-HSA were not influence the percentage of cell viability so much compared with the untreated cell (Fig. 7). Even concentration up to 500 μg mL^{-1}, the cell viability still over 80% indicating both nanoparticles were categorized as nontoxic materials.

3.5. Confocal Laser Scanning assessment

Further assessment using CLSM explore potential application of the designed CDs for cancer staining material. On Fig. 8, the green fluorescence of CDs after 1 h were appeared on the cytoplasm of HeLa tumor cell after it was exposed with Argon laser at 488 nm and photomultiplier tube (PMT) detector collects the fluorescent signal at range 498–550 nm.

Lower diameter of CDs makes it easy to pass the cell membrane via passive targeting process. Moreover, compared with bare CDs, encapsulation CDs with HSA increase the existence of CDs on the cytoplasm of the cell indicating with increasing fluorescent signal on CDs. Even the encapsulation made diameter of the nanoparticle become higher, HSA drives significantly the CDs to reach the tumor cell. High affinity of HSA to interacts with SPARC and the gp60 transcytosis on surface membrane of the cell and resulting active targeting way. The abundance of gp60 overexpressing on mostly surface of cancer cells were reported as good HSA receptor to initiate insertion process of the nanoparticles to the cell [43,44]. Z stacking mode on CLSM also used to prove both the CDs and CDs-HSA on the cytoplasm of the cell (Fig. 9).

We speculate to say that the accumulation of CDs-HSA on the cell is a package of active targeting and endocytosis process to make it exists on cell cytoplasm. On support this statement, the CLSM assessment of HeLa cell treated with CDs-HSA and incubated at temperature of 4°C for 1 h was carried out (Fig. 10). It is well documented that the mechanism of

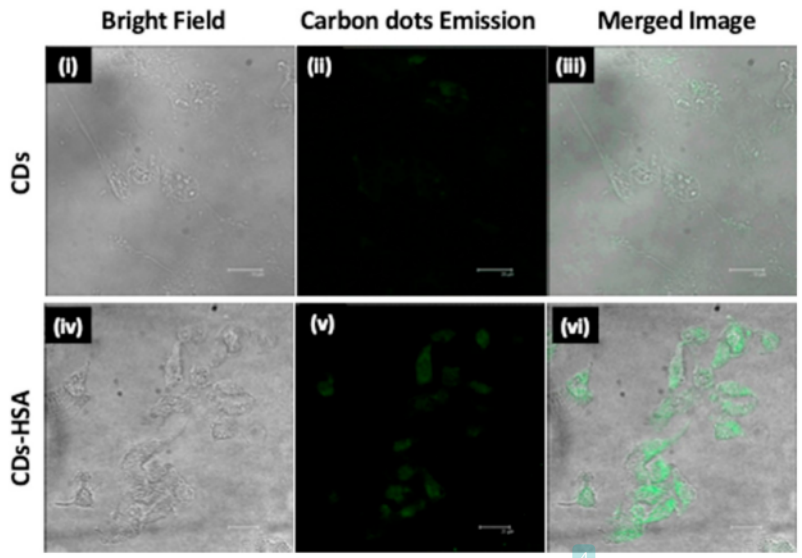

Fig. 8. CLSM images of HeLa cells after 1 h treated with CDs (i-iii) and CDs-HSA (iv-vi). HeLa cells imaged by excitation at 488 nm.

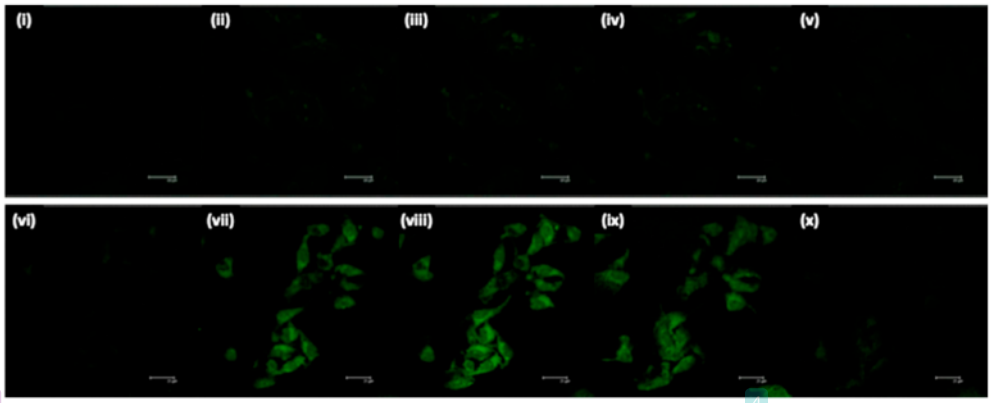

Fig. 9. CLSM images of HeLa cells using z-stacking mode after 1 h treated with CDs (i–v) and CDs-HSA (vi-x). HeLa cells imaged by excitation at 488 nm.

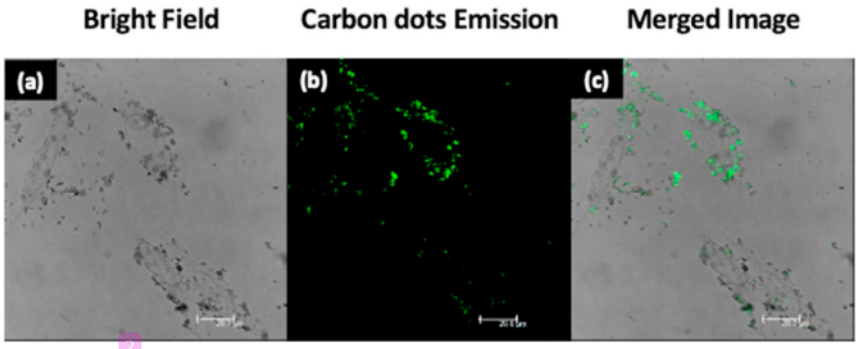

Fig. 10. CLSM images of HeLa cells After incubated with CDs-HSA on 4 °C for 1 h.

endocytosis is energy dependent and then, at low temperature, the cell metabolism is close on the stack condition [45,46]. Therefore, any outer materials cannot pass through the cell membrane for further endocytosis process. This Fig. 10 can be good data on proving that the CDs-HSA has attraction on the surface of membrane and enter the cell through endocytosis, where, at 4°C treatment of cell, the emission of CDs-HSA is presence on the membrane of cell.

4. Conclusion

We have developed a facile synthesize hydrophobic CDs by carbonization process. The surface modifications of CDs by HSA molecules (CDs-HSA) can phase transferring this nanomaterial to aqueous phase. These modified CDs were non-toxic and stable against physical condition of wide pH range and ionic strength. The analysis results indicated that CDs-HSA could be staining agent to detect the cancer cell via both active and passive targeting partway. The proposed CDs-HSA technique can inspire the development of novel approaches for the next preparation of multimodal nanoparticles for various applications in the future.

Declaration of competing interest

The authors declare that they have no known competing financial interests or personal relationships that could have appeared to influence the work reported in this paper.

Acknowledgements

The authors thank to Universitas Airlangga, Southeast Asia Taiwan University (SATU) forum and Ministry of Research, Technology, and Higher Education, Republic of Indonesia for financial support on Competence-based research project under contract no. 4/E1/KP. PTNBH/2019.

Appendix A. Supplementary data

Supplementary data to this article can be found online at https://doi.org/10.1016/j.matchemphys.2019.122266.

References

[1] B. Godin, E. Tasciotti, X. Liu, R.E. Serda, M. Ferrari, Multistage nanovectors: from concept to novel imaging contrast agents and therapeutics, Acc. Chem. Res. 44 (2011) 979–989.
[2] B. Wu, H. Wang, J. Chen, X. Yan, Fluorescence resonance energy transfer inhibition assay for α-fetoprotein excreted during cancer cell growth using functionalized persistent luminescence nanoparticles, J. Am. Chem. Soc. 133 (2011) 686–688.
[3] H. Li, X. He, Y. Liu, Z. Kang, One-step ultrasonic synthesis of water-soluble carbon nanoparticles with excellent photoluminescent properties, Carbon N. Y. 49 (2010) 605–609.
[4] C. Liu, P. Zhang, F. Tian, W. Li, F. Li, W. Liu, One-step synthesis of surface passivated carbon nanodots by microwave assisted pyrolysis for enhanced multicolor photoluminescence and bioimaging, J. Mater. Chem. 21 (2011) 13163–13167.
[5] J. Shen, Y. Zhu, X. Yang, C. Li, Graphene quantum dots: emergent nanolights for bioimaging, sensors, catalysis and photovoltaic devices, Chem. Commun. 48 (2012) 3686–3699.
[6] J. Gong, X. An, X. Yan, A Novel Rapid and Green Synthesis of Highly Luminescent Carbon Dots with Good Biocompatibility for Cell Imaging, vol. 1, 2014, pp. 1376–1379.
[7] S.N. Baker, B.A. Gary, Luminescent carbon nanodots: emergent nanolights, Angew. Chem. 49 (2010) 6726–6744.
[8] S. Dey, A. Govindaraj, K. Biswas, C.N.R. Rao, Luminescence properties of boron and nitrogen doped graphene quantum dots prepared from arc-discharge-generated doped graphene samples, Chem. Phys. Lett. (2014) 203–208, 595–596.
[9] L. Bao, Z. Zhang, Z. Tian, L. Zhang, C. Liu, Y. Lin, B. Qi, D.-W. Pang, Electrochemical tuning of luminescent carbon nanodots: from preparation to luminescence mechanism, Adv. Mater. 23 (2011) 5801–5806.
[10] H.P.S. Castro, V.S. Souza, J.D. Scholten, J.H. Dias, J.A. Fernandes, F. S. Rodembusch, R. dos Reis, J. Dupont, S.R. Teixeira, R.R.B. Correia, Synthesis and characterisation of fluorescent carbon nanodots produced in ionic liquids by laser ablation, Chem. Eur J. 22 (2016) 138–143.
[11] F. Wang, S. Pang, L. Wang, Q. Li, One-step synthesis of highly luminescent carbon dots in noncoordinating solvents, Chem. Mater. 22 (2010) 4528–4530.
[12] Z. Yongqiang, L. Xingyuan, F. Yi, G. Xiaoyang, Z. Lei, L. Ying, L. Jie, One step microwave synthesis of N-doped hydroxyl-functionalized carbon dots with ultra-high fluorescence quantum yields, Nanoscale 8 (2016) 15281–15287.
[13] A. Talib, S. Pandey, M. Thakur, H. Wu, Synthesis of highly fluorescent hydrophobic carbon dots by hot injection method using Paraplast as precursor, Mater. Sci. Eng. C 48 (2015) 700–703.
[14] H. Ming, Z. Ma, Y. Liu, K. Pan, H. Yu, F. Wang, Z. Kang, Large scale electrochemical synthesis of high quality carbon nanodots and their photocatalytic property, Dalton Trans. 41 (2012) 9526–9531.
[15] Y. Dong, J. Shao, C. Chen, H. Li, R. Wang, Y. Chi, X. Lin, G. Chen, Blue luminescent graphene quantum dots and graphene oxide prepared by tuning the carbonization degree of citric acid, Carbon N. Y. 50 (2012) 4738–4743.
[16] M.Z. Fahmi, W. Sukmayani, S.Q. Khairunisa, A.M. Witaningrum, D.W. Indriati, M. Q.Y. Matondang, J.-Y. Chang, T. Kotakie, M. Kameoka, Design of boronic acid-attributed carbon dots on inhibits HIV-1 entry, RSC Adv. 6 (2016) 92996–93002.
[17] R. Liu, D. Wu, X. Feng, Bottom-up fabrication of photoluminescent graphene quantum dots with uniform morphology, J. Am. Chem. Soc. 133 (2011) 15221–15223.
[18] M.Z. Fahmi, J.Y. Chang, A facile strategy to enable nanoparticles for simultaneous phase transfer, folate receptor targeting, and cisplatin delivery, RSC Adv. 4 (2014) 56713–56721.
[19] V. Gude, Synthesis of hydrophobic photoluminescent carbon nanodots by using L-tyrosine and citric acid through a thermal, Beilstein J. Nanotechnol. 5 (2014) 1513–1522.
[20] C. Ding, A. Zhu, Y. Tian, Functional surface engineering of c-dots for fluorescent biosensing and in vivo bioimaging, Acc. Chem. Res. 47 (2014) 20–30.
[21] M.Z. Fahmi, K. Ou, J. Chen, M. Ho, S. Tzing, J. Chang, Development of bovine serum albumin-modified hybrid nanoclusters for magnetofluorescence imaging and drug delivery, RSC Adv. 4 (2014) 32762–32772.
[22] A. Angelini, J. Morales-sanfrutos, P. Diderich, S. Chen, C. Heinis, Bicyclization and tethering to albumin yields long-acting peptide antagonists, J. Med. Chem. 55 (2012) 10187–10197.
[23] B. Zhang, X. Wang, F. Liu, Y. Cheng, D. Shi, Effective reduction of nonspecific binding by surface engineering of quantum dots with bovine serum albumin for cell-targeted imaging, Langmuir 28 (2012) 16605–16613.
[24] F. Yang, Y. Zhang, H. Liang, Interactive association of drugs binding to human serum albumin, Int. J. Mol. Sci. 15 (2014) 3580–3595.
[25] Z. Sheng, D. Hu, M. Zheng, P. Zhao, H. Liu, D. Gao, P. Gong, G. Gao, P. Zhang, Y. Ma, L. Cai, Smart human serum albumin-indocyanine green nanoparticles generated by programmed assembly for dual-modal imaging-guided cancer synergistic phototherapy, ACS Nano 8 (2014) 12310–12322.
[26] N. Desai, V. Trieu, Z. Yao, L. Louie, S. Ci, A. Yang, C. Tao, T. De, B. Beals, D. Dykes, P. Noker, R. Yao, E. Labao, M. Hawkins, P. Soon-Shiong, Increased antitumor activity, intratumor paclitaxel concentrations, and endothelial cell transport of cremophor-free, albumin-bound paclitaxel, ABI-007, compared with cremophor-based paclitaxel, Clin. Cancer Res. 12 (2006).
[27] C. Jiang, H. Cheng, A. Yuan, X. Tang, J. Wu, Y. Hu, Hydrophobic IR780 encapsulated in biodegradable human serum albumin nanoparticles for photothermal and photodynamic therapy, Acta Biomater. 14 (2014) 61–69.
[28] J. Look, N. Wilhelm, H. Von Briesen, N. Noske, C. Günther, L. Klaus, G. Erwin, Ligand-modified human serum albumin nanoparticles for enhanced gene delivery, Mol. Pharm. 12 (2015) 3202–3213.
[29] L. Liu, Y. Bi, M. Zhou, X. Chen, X. He, Y. Zhang, T. Sun, C. Ruan, Q. Chen, H. Wang, C. Jiang, Biomimetic human serum albumin nanoparticle for efficiently targeting therapy to metastatic breast cancers, ACS Appl. Mater. Interfaces 9 (2017) 7424–7435.
[30] S.K. Bhunia, A. Saha, A.R. Maity, S.C. Ray, N.R. Jana, Carbon nanoparticle-based fluorescent bioimaging probes, Sci. Rep. 3 (2013) 1473–1480.
[31] Z. Fan, L. Shuhua, Y. Fanglong, F. Louzhen, Fluorescent graphene quantum dots for biosensing and bioimaging, RSC Adv. 5 (2015) 19773–19789.
[32] M.I. Chavez-bejar, J.L. Báez-viveros, A. Martínez, F. Bolívar, G. Gosset, Biotechnological production of L -tyrosine and derived compounds, Process Biochem. 47 (2012) 1017–1026.
[33] M.J. Krysmann, A. Kelarakis, P. Dallas, E.P. Giannelis, Formation mechanism of carbogenic nanoparticles with dual photoluminescence emission, J. Am. Chem. Soc. 1550 (2012) 1–4.
[34] S. Sahu, B. Behera, T.K. Maiti, S. Mohapatra, Simple one-step synthesis of highly luminescent carbon dots from orange juice: application as excellent bio-imaging agents, Chem. Commun. 48 (2012) 8835–8837.
[35] B. De, K. Niranjan, A green and facile approach for the synthesis of water, RSC Adv. 3 (2013) 8286–8290.
[36] S. Chandra, P. Patra, S.H. Pathan, S. Roy, S. Mitra, A. Layek, R. Bhar, P. Pramanik, A. Goswami, Luminescent S-doped carbon dots: an emergent architecture for multimodal applications, J. Mater. Chem. B 1 (2013) 2375–2382.
[37] J. Gu, M.J. Hu, Q.Q. Guo, Z.F. Ding, X.L. Suna, J. Yang, High-yield synthesis of graphene quantum dots with strong green photoluminescence, RSC Adv. 4 (2014) 50141–50144.
[38] M. D, D.C. Carter, F. Rüker, The three recombinant domains of human serum albumin. Structural characterization and ligand binding properties, J. Biol. Chem. 274 (1999) 29303–29310.
[39] M.Z. Fahmi, A. Haris, A.J. Permana, D.L.N. Wibowo, B. Purwanto, Y.L. Nikmah, A. Idris, Bamboo leaf-based carbon dots for efficient tumor imaging and therapy, RSC Adv. 8 (2018) 38376–38383.

[40] Y.-M. Long, C.-H. Zhou, Z.-L. Zhang, Z.-Q. Tian, L. Bao, Y. Lina, D.-W. Pang, Shifting and non-shifting fluorescence emitted by carbon nanodots, J. Mater. Chem. 22 (2012) 5917–5920.
[41] A.O. Elzoghby, W.M. Samy, N.A. Elgindy, Albumin-based nanoparticles as potential controlled release drug delivery systems, J. Control. Release 157 (2012) 168–182.
[42] M.Z. Fahmi, J. Chang, Forming double layer-encapsulated quantum dots for bio-imaging and cell targeting, Nanoscale 5 (2013) 1517–1528.
[43] S. Ichimizu, H. Watanabe, H. Maeda, K. Hamasaki, Y. Nakamura, V.T.G. Chuang, Y. Ishima, Design and tuning of a cell-penetrating albumin derivative as a versatile nanovehicle for intracellular drug delivery, J. Control. Release 277 (2018) 23–34.
[44] T.Y. Tu, S.J. Yang, M.H. Tsai, C.H. Wang, S.Y. Lee, T.H. Young, M.J. Shieh, Dual-triggered drug-release vehicles for synergistic cancer therapy, Colloids Surfaces B Biointerfaces 173 (2019) 788–797.
[45] K. Kostarelos, L. Lacerda, G. Pastorin, W. Wu, S. Wieckowski, J. Luangsivilay, S. Godefroy, D. Pantarotto, J.-P. Briand, S. Muller, M. Prato, A. Bianco, Cellular uptake of functionalized carbon nanotubes is independent of functional group and cell type, Nat. Nanotechnol. 2 (2007) 108–113.
[46] K. Shojima, A. Sato, H. Hanaki, I. Tsujimoto, M. Nakamura, K. Hattori, Y. Sato, K. Dohi, M. Hirata, H. Yamamoto, A. Kikuchi, Wnt5a promotes cancer cell invasi on and proliferation by receptor-mediated endocytosis-dependent and-independent mechanisms, respectively, Sci. Rep. 5 (2015), 8042-8034.

Human serum albumin capsulated hydrophobic carbon nanodots as staining agent on HeLa tumor cell

ORIGINALITY REPORT

8%	2%	8%	3%
SIMILARITY INDEX	INTERNET SOURCES	PUBLICATIONS	STUDENT PAPERS

PRIMARY SOURCES

1	Nicolò Mauro, Mara Andrea Utzeri, Salvatore Emanuele Drago, Aldo Nicosia, Salvatore Costa, Gennara Cavallaro, Gaetano Giammona. "Hyaluronic acid dressing of hydrophobic carbon nanodots: A self-assembling strategy of hybrid nanocomposites with theranostic potential", Carbohydrate Polymers, 2021 Publication	1%
2	Aswandi Wibrianto, Siti Q. Khairunisa, Satya C. W. Sakti, Yatim L. Ni'mah, Bambang Purwanto, Mochamad Z. Fahmi. "Comparison of the effects of synthesis methods of B, N, S, and P-doped carbon dots with high photoluminescence properties on HeLa tumor cells", RSC Advances, 2021 Publication	1%
3	Wahyu Widanarto, Ananda Iqbal Ekaputra, Mukhtar Effendi, Wahyu Tri Cahyanto et al. "Neodymium ions activated barium ferrite composites for microwave X-band absorber	1%

applications: Synthesis and characterizations", Composites Communications, 2020
Publication

4	Fahmi, Mochamad Zakki, Jem-Kun Chen, Chih-Ching Huang, Yong-Chien Ling, and Jia-Yaw Chang. "Phenylboronic acid-modified magnetic nanoparticles as a platform for carbon dot conjugation and doxorubicin delivery", Journal of Materials Chemistry B, 2015. Publication	1 %
5	Bibekananda De, Niranjan Karak. "A green and facile approach for the synthesis of water soluble fluorescent carbon dots from banana juice", RSC Advances, 2013 Publication	1 %
6	Chun-Yi Cheng, Keng-Liang Ou, Wei-Ting Huang, Jem-Kun Chen, Jia-Yaw Chang, Cheng-Hsien Yang. " Gadolinium-Based CuInS /ZnS Nanoprobe for Dual-Modality Magnetic Resonance/Optical Imaging ", ACS Applied Materials & Interfaces, 2013 Publication	1 %
7	www.nature.com Internet Source	1 %
8	Mochamad Zakki Fahmi, Keng-Liang Ou, Jem-Kun Chen, Ming-Hua Ho, Shin-Hwa Tzing, Jia-Yaw Chang. "Development of bovine serum	1 %

albumin-modified hybrid nanoclusters for magnetofluorescence imaging and drug delivery", RSC Adv., 2014
Publication

9	Yu-Yu Aung, Aswandi Wibrianto, Jefry S. Sianturi, Desita K. Ulfa et al. "Comparison Direct Synthesis of Hyaluronic Acid-Based Carbon Nanodots as Dual Active Targeting and Imaging of HeLa Cancer Cells", ACS Omega, 2021 Publication	1 %
10	onlinelibrary.wiley.com Internet Source	1 %

Exclude quotes	On	Exclude matches	< 1%
Exclude bibliography	On		

Human serum albumin capsulated hydrophobic carbon nanodots as staining agent on HeLa tumor cell

GRADEMARK REPORT

FINAL GRADE

/0

GENERAL COMMENTS

Instructor

PAGE 1

PAGE 2

PAGE 3

PAGE 4

PAGE 5

PAGE 6

PAGE 7

PAGE 8

PAGE 9